Published in final edited form as:
Biochemistry. 2012 February 28; 51(8): 1586–1597. doi:10.1021/bi201575f.

THE ROLE OF CALCIUM IN METALLOENZYME: EFFECTS OF CALCIUM REMOVAL ON THE AXIAL LIGATION GEOMETRY AND MAGNETIC PROPERTIES OF THE CATALYTIC DIHEME CENTER IN MauG†

Yan Chen[Δ], **Sunil G. Naik**[Δ], **J. Krzystek**[§], **Sooim Shin**[¶], **William H. Nelson**[‡], **Shenghui Xue**[&], **Jenny. J. Yang**[Δ], **Victor L. Davidson**[¶], and **Aimin Liu**[*,Δ]

[Δ]Department of Chemistry, Molecular Basis of Disease Program, Georgia State University, P.O. Box 4098, Atlanta, GA 30303

[&]Department of Biology, Molecular Basis of Disease Program, Georgia State University, P.O. Box 4098, Atlanta, GA 30303

[‡]Department of Physics and Astronomy, Molecular Basis of Disease Program, Georgia State University, P.O. Box 4098, Atlanta, GA 30303

[¶] Burnett School of Biomedical Sciences, College of Medicine, University of Central Florida, Orlando, FL 32827

[§]National High Magnetic Field Laboratory, Florida State University, Tallahassee, FL 32310

Abstract

MauG is a diheme enzyme possessing a five-coordinate high-spin heme with an axial His ligand and a six-coordinate low-spin heme with His-Tyr axial ligation. A Ca^{2+} ion is linked to the two hemes via hydrogen-bond networks, and the enzyme activity depends on its presence. Removal of Ca^{2+} alters the EPR signals of each ferric heme such that the intensity of the high-spin heme was decreased and the low-spin heme was significantly broadened. Addition of Ca^{2+} back to the sample restored the original EPR signals and enzyme activity. The molecular basis for this Ca^{2+}-dependent behavior was studied by magnetic spectroscopy. The results show that in the Ca^{2+}-depleted MauG the high-spin heme was converted to low-spin and the original low-spin heme exhibited a change in relative orientations of its two axial ligands. The properties of these two hemes are each different than in native MauG and are now similar to each other. The EPR spectrum of Ca^{2+}-free MauG appears to describe one set of low-spin ferric heme signals with a large g_{max} and g-anisotropy and a greatly altered electromagnetic relaxation property. Both EPR and Mössbauer spectroscopic results show that the two hemes are present as unusual highly axial low-spin (HALS)-like hemes in Ca^{2+}-depleted MauG, with a smaller orientation angle between the two axial ligand planes. These findings provide insight into the correlation of the enzyme

†This work was supported by NSF Grant MCB-0843537 (AL), NIH grants GM041574 (VLD) and GM081749 (JJY), Georgia State University pre-doctoral fellowships (YC & SX), and Georgia Cancer Coalition Distinguished Scientist Program (AL).

* Address correspondence to: Aimin Liu, Departments of Chemistry, Georgia State University, P. O. Box 4098, Atlanta, GA, 30303. Telephone: (404) 413-5532; Fax: (404) 413-5505; Feradical@gsu.edu..

TEXTURAL FOOTNOTES

This paper is dedicated to the memory of the coauthor Professor William H. Nelson who died from a heart attack on the 19th December 2010.

Supporting Information Available. Figures S1 and further details of the proton NMR relaxometry study. This material is available free of charge via the Internet at http://http://pubs.acs.org.

activity with the orientation of axial heme ligands, and describe a role for the calcium ion in maintaining this structural orientation that is required for activity.

It is widely recognized that Ca^{2+} ions are central to complex intracellular messenger systems that mediate a broad range of biological processes: muscle contraction, secretion, glycolysis and gluconeogenesis, ion transport, cell division and growth (*1*). For instance, there are a number of proteins belonging to the calmodulin superfamily which are known to be intracellular Ca^{2+}-triggered proteins (*2, 3*). Calcium ion is found to regulate enzymes such as protein kinase C (*4*), phospholipase A_2 (*5*), α-amylase (*6*), and nucleases by binding at or near the active site to control their catalytic functions (*7*). Most endothelial and neuronal nitric oxide synthases are Ca^{2+}-dependent for producing nitric oxide (*8*). Ca^{2+} binding in proximity to catalytic hemes is also reported in *b*-type heme peroxidases and *c*-type diheme peroxidases. The function of Ca^{2+} in bacterial diheme protein cytochrome *c* peroxidase (CcP) has been postulated as maintenance of the heme conformation, rearrangement of the internal hydrogen bond network, modulation of the electron transfer rates between the two domains of the protein (*9*), and it also affects the electrochemical behavior of the two hemes (*10*). It is important to understand the molecular mechanism by which calcium is used in regulation of metalloenzymes.

MauG is a *c*-type diheme enzyme that exhibits sequence and structural homology to bacterial diheme CcP enzymes (*11*, *12*). However, MauG does not function as a cytochrome c peroxidase; instead MauG uses H_2O_2 to catalyze posttranslational modifications of its protein substrate (*13*). The chemical reaction mediated by MauG is an unusual six-electron oxidation required for conversion of a precursor of methylamine dehydrogenase (preMADH) to its catalytically active form which contains a protein-derived tryptophan tryptophylquinone (TTQ) cofactor (*14*, *15*). The crystal structure of the MauG-preMADH complex reveals the presence of a Ca^{2+} ion in proximity to the two hemes (Figure 1) (*12*). The orientation of the Ca^{2+} and two hemes in MauG is similar to that in the CcPs. Ca^{2+} binding is associated with conversion of the enzyme from an inactive diferric form to an active mixed-valence form. In contrast, the Ca^{2+} of MauG does not readily dissociate or appear to play a regulatory role in the catalytic cycle. It was previously shown that MauG exhibited altered absorption and resonance Raman spectra and was no longer able to catalyze TTQ biosynthesis after extensive treatment with Ca^{2+} ion chelators (*16*). After addition of Ca^{2+} to the Ca^{2+}-depleted MauG, full TTQ biosynthesis activity and reactivity towards H_2O_2 was restored, and the spectral properties returned to those of native MauG. The circular dichroism spectra of native and Ca^{2+}-depleted MauG were essentially the same, consistent with Ca^{2+}-induced conformational changes involving domain or loop movements rather than general unfolding or alteration of secondary structure (*16*).

The crystal structure of the MauG-preMADH protein complex reveals that the two ferric ions of the hemes are 21 Å apart. The five-coordinate high-spin ferric heme, which reacts with H_2O_2 to generate a catalytic *bis*-Fe(IV) intermediate (*17*), is positioned over 40 Å from the two substrate tryptophan residues of preMADH. Residue Trp93 and a Ca^{2+} ion are both positioned between the two hemes (*12*). The Ca^{2+} ion in MauG, about 12 Å from each Fe ion, is coordinated by seven oxygen atoms from the carboxyl oxygen of Asn66, the amide carboxyl oxygens of Pro277 and Thr275, and four well-ordered structural water molecules (Figure 1). Propionate substituents of both hemes of MauG are linked to the Ca^{2+} ion via hydrogen bonded water molecules. Previous results indicate that the presence of Ca^{2+} is critical in maintaining an appropriate structural environment for the hemes, which allows MauG to generate the unprecedented *bis*-Fe(IV) intermediate and catalyze a complex six-electron oxidation of a protein substrate (*16*, *17*). However, how the Ca^{2+} ion helps to organize the catalytic di-iron center and maintain the functionally active state remains

unknown. Thus far it has not been possible to crystallize the inactive Ca^{2+}-depleted MauG. In this study X-band and high-field EPR (HFEPR) spectroscopy, proton relaxometry, and Mössbauer spectroscopy are used to characterize the structure and unusual magnetic properties of the hemes in Ca^{2+}-depleted MauG. The results reveal a significant, reversible, Ca^{2+}-dependent change in the nature and orientation of the axial ligands of the two hemes, which profoundly influences the axial ligation geometry and magnetic properties of both hemes. This is a previously unreported role for calcium ion in maintaining the proper heme orientations that are required for activity.

Experimental Procedures

Protein preparation

The preparation of MauG has been described elsewhere (*11*). The concentration of MauG was calculated using the extinction coefficient of the Soret band of the heme groups (ε_{406} = 309,000 $M^{-1}cm^{-1}$) (*18*). Ca^{2+}-depleted MauG was prepared by incubating 10 mM EDTA or EGTA with native MauG at 4 °C overnight and then desalting the protein by a pre-packed G-25 column from GE Healthcare in 50 mM potassium phosphate buffer, pH 7.5. Ca^{2+}-depleted MauG was reconstituted with Ca^{2+} by changing the potassium phosphate buffer of Ca^{2+}-depleted MauG into 50 mM Tris buffer, pH 7.5 followed by overnight incubation with 10 mM calcium chloride at 4 °C. Free metal ions were removed by running through the samples at a 5-ml HiTrap™ Desalting Column (GE Healthcare, NJ).

X-band EPR spectroscopy

The continuous-wave X-band EPR spectra were recorded at liquid helium temperatures on a Bruker ER200D spectrometer at 100-kHz modulation frequency using a 4116DM resonator. Sample temperature was maintained by an ITC503S controller, an ESR910 cryostat and a LLT650/13 liquid helium transfer tube (Oxford Instruments, Concord, MA). EPR simulations were performed using the EPR simulation program SPIN (*19*). The EPR relaxation behavior of the ferric hemes was characterized by the parameters of the saturation curves in terms of the microwave power at half saturation $P_{1/2}$ and b, which describes the contribution of inhomogeneous broadening according to eq 1 (*20*-*22*):

$$I \propto \frac{I_0}{(1+P/P_{1/2})^{b/2}} \quad (1)$$

where I was the EPR derivative signal amplitude (peak-to-peak height) and P is the microwave power. It is known that dipole coupling can lead to significant errors in the determination of spin-relaxation times (*20*). However, the two heme Fe ions in MauG are 21 Å apart. The dipolar-dipolar interactions are not detectable in any significant degree. Thus, eq 1 was applicable to MauG.

High-field EPR

HFEPR spectra were recorded at the EMR Facility at the National High Magnetic Field Laboratory (NHMFL), Tallahassee, Florida (*23*). A Virginia Diodes (Charlottesville, VA) source operating at a base frequency of 12 – 14 GHz and multiplied by a cascade of multipliers was used in conjunction with a 15/17 tesla superconducting magnet. Detection was provided with an InSb hot-electron bolometer (QMC Ltd., Cardiff, UK). The magnetic field was modulated at 50 kHz. A Stanford Research Systems SR830 lock-in amplifier converted the modulated signal to DC voltage. Low temperature was provided by an Oxford Instruments (Oxford, UK) continuous flow cryostat and a temperature controller from the same source.

Mössbauer Spectroscopy

^{57}Fe-enriched native MauG was prepared from a previously described procedure (*17*) with minor modifications. Briefly, the LB medium was passed through a Chelex-100 resin. The ^{57}Fe stock solution was prepared by dissolving ^{57}Fe metal-powder (95.4% of ^{57}Fe enrichment, Science Engineering & Education Co.) in 2.5 M H_2SO_4 under anaerobic condition. The iron and acid mixture was incubated at 60 °C while stirring in an anaerobic chamber until the ^{57}Fe metal was completely dissolved in the acid. The ^{57}Fe solution (0.72 M) was added to the Chelex-100 treated LB medium to a final concentration for 80 M for preparation of the cell culture. The ^{57}Fe-enriched native MauG and ^{57}Fe-enriched Ca^{2+}-depleted MauG were (1 mM, 400 μL, isolated from 60 L cell culture for each sample) were transferred into delrin cups and subjected for Mössbauer analyses frozen. Mössbauer spectra were recorded in a weak-field spectrometer equipped with a Janis 8DT variable-temperature cryostat at Emory University. The zero velocity of the spectra refers to the centroid of a room-temperature spectrum of a metallic iron foil.

Proton NMR relaxometry

T_1 and T_2 of the native MauG and Ca^{2+}-depleted MauG was measured on a Bruker Minispec mq60 NMR Analyzer at 4°C. Native and Ca^{2+}-depleted MauG samples (at 150 M concentration) were placed in quartz tube respectively and applied to measure the relaxation time. The r_1 and r_2 are calculated by the following equations:

$$r_1 = \left(\frac{1}{T_1} - \frac{1}{T_{1buffer}}\right) / [\text{heme}] \quad (2)$$

$$r_2 = \left(\frac{1}{T_2} - \frac{1}{T_{2buffer}}\right) / [\text{heme}] \quad (3)$$

Results

EPR spectroscopy

The low temperature X-band EPR spectrum of native MauG shows three ferric heme species (Figure 2A): (i) a high-spin (S = 5/2) heme with g values of 1.99 and a 5.57 that can be assigned to the five-coordinate (5C) His-ligated heme (designated HS heme hereafter), (ii) a low-spin (S = 1/2) heme with g values of 1.87, 2.19, and 2.54 which is assigned to the six-coordinate (6C) His-Tyr ligated heme (designated LS heme hereafter), and (iii) a second broad and low-intensity low-spin (S = 1/2) heme observed at g values 1.52, 2.32, and 2.89, which is derived from the high-spin heme upon freezing (*11*). The HS and LS hemes have been previously shown to exhibit distinct relaxation properties, with the LS heme more easily saturated by the applied microwave power. The EPR spectrum of native MauG, shown in Figure 2A, was obtained at 10 K with 1 mW microwave power. This was found to be the optimal condition to observe both the HS and LS hemes in MauG. Upon relatively extensive treatment with EDTA or EGTA (while maintaining protein stability, see Experimental Procedures), MauG's catalytic activity is nearly lost, and its absorption and resonance Raman spectra are altered (*16*). In the EPR spectrum of the Ca^{2+}-depleted MauG (Figure 2B) most of the original HS and LS ferric heme EPR signals disappear. The remaining signals are of less than 10% of their orginal intensity and likely arise from a subpopulation of residual native MauG from which Ca^{2+} was not completely removed after extensive EDTA/EGTA treatment. A single new low-spin heme EPR signal (g values of 1.52, 2.27, and 2.97) appears in the Ca^{2+}-depleted MauG spectrum, which is broader and of much lower intensity than the original LS ferric heme EPR signal (designated as LS* heme

hereafter). Due to its low amplitude, this new LS* EPR signal can be easily underestimated, leading to a proposition that the diferric hemes changed from the EPR-active states to what appears to be an EPR-inactive state in the X-band EPR spectrum (Figure 2). When the Ca^{2+}-depleted MauG sample was reconstituted with Ca^{2+}, the EPR signals returned to those of the original native MauG (Figure 2C). Thus, this apparent loss of EPR signal intensities from the two ferric hemes, caused by depletion of Ca^{2+}, is a reversible process which affects the catalytic activity of MauG.

While it is apparent the EPR signal intensity of the HS ferric heme decreased in the Ca^{2+}-depleted MauG sample, the LS heme appeared to become noticeably broadended. The *g*-anisotropy (g_x - g_z) of the LS heme is 0.67. This value is 1.37 for LS* after depletion of Ca^{2+}. The broad LS* species spans over nearly 300 millitesla in the EPR spectrum. Unlike the HS heme EPR signal, the LS and LS* species cannot be directly quantitated from their EPR signals because of overlapping resonances in the spectrum. To circumvent the quantitation difficulty, we performed EPR simulations. We were able to simulate both the LS and LS* species. The theoretically reconstructed EPR spectrum in the $g = 2$ region is shown in Figure 3. The results show that about 10% of the EPR signals were contributed from the original LS ferric heme.

Since the *c*-type hemes of MauG are covalently bound, this apparent loss of the EPR signal amplitude upon Ca^{2+} depletion is unlikely due to loss of heme. After the metal chealtor treatment, the enzyme was desalted through a column. With addition of Ca^{2+}, but not iron ion, the EPR signals re-emerged. It is also unlikely that the ferric hemes are converted to EPR-silent redox states, such as Fe(II) or Fe(IV), by treatment with the metal chelators. This leaves two other plausible possibilities which may lead to the significant reduction of amplitude of the ferric heme EPR signals. One is that the two ferric ions ($S = 1/2$ and $S = 5/2$, respectively) become spin-coupled to produce a non-Kramers integer ground spin state ($S = 2$ or 3), which is typically not accessible by conventional X-band EPR due to a large zero-field splitting. A second possibility is that the electron spin resonance and magnetic relaxation properties of the ferric hemes have changed considerably such that their EPR signals are broadened, resulting in substantial reductions in the signal amplitudes that are much lower than those in the native MauG at the given microwave power. To test these possibilities and to determine the structural basis for the observed changes in the electronic properties in the upon Ca^{2+}-depleted MauG, Mössbauer and multifrequency EPR spectroscopy as well as proton relaxivity measurements were employed to probe the status of the heme iron ions in the native and Ca^{2+}-depleted MauG samples.

High-field EPR spectroscopy

To more precisely characterize the difference in the properties of ferric LS heme of native MauG and LS* heme of Ca^{2+}-depleted MauG, their EPR spectra were recorded in high field where the differences become more apparent and *g*-anisotropy typically becomes better resolved (Figure 4). These spectra are dominated by fast-passage effects, resulting in their absorptive shape, rather than the standard first-derivative shape. The 104 GHz spectrum of the native form of MauG was simulated as a superposition of two low-spin ferric ions characterized by *g*-matrices almost identical to those determined from X-band measurements. The major species is the original LS ferric heme with $g = 1.87, 2.19, 2.54$ with a linewidth of ca. 75 G. The other species is the low-spin ferric heme derived from the high-spin heme site upon freezing with $g = 1.52, 2.32, 2.89$ and a larger anisotropic linewidth of between 200 and 400 G. The HS heme is also visible with low intensity in the HFEPR spectrum due to difference in relaxation properties. The HFEPR spectrum of Ca^{2+}-depleted MauG was simulated as a superposition of two low-spin ferric ions. One is attributed to the LS heme of residual native MauG. Given the relatively high affitnity of MauG for Ca^{2+} it was difficult to completely deplete Ca^{2+} and prevented it from being

scavenged by the apo form from trace amounts of Ca^{2+} in the buffer. The other species is that of the LS* heme characterized by g = 1.50, 2.27, 2.97 and by large anisotropic linewidth of 200–400 G. As this signal accounts for nearly all the ferric heme present, it represents two low-spin heme centers with similar magnetic properties which were derived from the original HS and LS hemes.

EPR spin relaxation properties

The low EPR signal amplitude of the LS* relative to the heme signals in native MauG suggests that the conversion to LS* may have affected the spin relaxation and power saturation behavior of the hemes. The HS and LS hemes of native MauG exhibit different half-power saturation values ($P_{1/2}$). We found that microwave power of 1 mW was the optimal power for obtaining a spectrum that clearly shows the spectra of the two ferric hemes of native MauG at 10 K. At higher power values, the LS ferric heme EPR signal became severely saturated, while at lower power values, the intensity of the HS ferric EPR signal was very weak. However, the Ca^{2+}-depleted MauG appeared to be EPR silent when a microwave power of 1 mW was used. Figure 5 shows EPR spectra for native and Ca^{2+}-depleted MauG where each was recorded using the most appropriate microwave power for observing multiple HS and LS species. The EPR signal intensity of LS* heme of Ca^{2+}-depleted MauG shown in Figure 5 which was taken with over one order of magnitude higher of microwave power (12.7 mW) is now comparable to ferric heme EPR intensity of native MauG of the same protein concentration recorded with 1 mW power and with otherwise the same temperature and instrument conditions. The total spins of LS* obtained at 12.7 mW accounts for nearly 90% of the total ferric ion of the two heme sites when compared to that in native MauG after integration of all EPR signals. The inset in Figure 5 shows the power saturation behavior of the new LS* species compared to that of the major LS ferric heme in native MauG. While the LS heme EPR signal becomes readily saturated when the microwave power approaches the milliwatt range, the power saturation profile of LS* is completely distinct and presents a $P_{1/2}$ value of 22.8 mW at 10 K. In contrast, the $P_{1/2}$ value of the LS species was 0.6 mW. The b values of LS and LS* were 0.96 and 1,3, respectively. These values suggest an inhomogeneous broadening of the EPR signals. The relative poor fitting of the power saturation profiles were due to the fact that the full saturation was not reached by the instrumentation used. The presumed weak dipolar couplings between the two Fe ions may also contribute to the spin relation and can lead to errors in the data analysis (*20*). This result indicates that the electron spin relaxations of the two hemes in the Ca^{2+}-depleted MauG are much faster than in the native MauG.

Mössbauer spectroscopy

Figure 6 (top panel) displays the Mössbauer spectra of the ^{57}Fe-enriched MauG and Ca^{2+}-depleted MauG recorded at 180 K. Only quadrupole doublets are observed in these spectra, which indicate that the electronic relaxation is faster than the nuclear precession at this temperature. On the basis of the EPR spectrum of native MauG, which shows the presence of three different heme species, the spectrum of native MauG (Figure 6) was accordingly least-squares fit with three quadrupole doublets. One of the doublets (top panel, A, red line) with parameters of ΔE_Q = 2.0 mm/s and δ = 0.45 mm/s is characteristic of a HS ferric heme and accounts for 25% of the total Fe. The other two doublets are characteristic of low-spin ferric hemes with parameters of ΔE_Q = 2.44 mm/s, δ = 0.27 mm/s (cyan line) and ΔE_Q = 2.09 mm/s, δ = 0.23 mm/s (green line). Together, both doublets account for 75% of the total Fe. The green doublet (55%) is assigned to the LS heme and the cyan doublet (20%) to the low-spin species derived from freezing of the HS heme. The 180-K Mössbauer spectrum of the Ca^{2+}-depleted MauG (B) is distinct from that of native MauG. The spectrum is sharper and shows apparently a smaller quadrupole splitting. In accord with the high-field EPR data of the Ca^{2+} depleted MauG, which show that a majority (~90%) of the Fe is present in the

LS* state, the Mössbauer spectrum was least-squares fit with a single asymmetric quadrupole doublet. The parameters obtained (E_Q = 2.17 mm/s, δ = 0.22 mm/s) are characteristic of low-spin ferric heme and the doublet is assigned to the LS* heme. The minor spectral component (~10%) arising from the residual native MauG is unresolved and therefore is not considered in our analysis. Due to the minor contributions, its presence is not expected to have a significant effect on the determination of the LS* heme parameters.

To obtain a more detailed description of the electromagnetic properties of these hemes and to investigate directly whether the two LS* heme moieties are spin-coupled in the Ca^{2+}-depleted MauG, Mössbauer spectra were also recorded at low temperature (4.2 K) in the presence of a weak external magnetic field of 50 mT parallel or perpendicular to the γ radiation (Figure 6, bottom panel). Magnetic hyperfine-split spectra are observed for both the native MauG (A) and Ca^{2+}-depleted MauG (B and C), indicating unambiguously that, similar to native MauG, the two heme groups in the Ca^{2+}-depleted MauG are not spin-coupled. Consistent with analysis applied to the 180-K spectra, the 4.2-K native MauG spectrum (A) is also decomposed into three spectral components arising from the HS ferric species (25%, red line), the LS ferric species (55%, green line), and the low-spin species derived from freezing of the HS heme (20%, cyan line). The Mössbauer and spin-Hamiltonian parameters of the HS and LS ferric species, listed in Table 1, are similar to those reported previously (*17*). The parameters for the low-spin species derived from freezing of the HS heme are obtained using the procedures described in the next paragraph and are also listed in Table 1.

The 4.2-K Ca^{2+}-depleted Mössbauer spectra (Figure 6 bottom panel, B and C) were simulated with a single low-spin ferric species, presumably the LS* species. To this end, we employed a crystal field theory (*24, 25*) that has been used successfully to analyze low-spin ferric heme Mössbauer spectra (*26*) to estimate the *A* tensor from the observed *g* values (2.97, 2.27 and 1.52). In general, the quadrupole splitting for low-spin ferric complexes is relatively temperature insensitive. The ΔE_Q value, 2.17 mm/s, obtained at 180 K was therefore used for the simulation of the 4.2-K spectra. Consequently, the only parameter that is varied in our simulation is the asymmetric parameter, η, which was varied until the simulation yielded theoretical spectra comparable with the experimental spectra. The solid lines plotted (90% of the total Fe absorption) over the experimental spectra (B and C) are results of theoretical simulation of LS* using the parameters listed in Table 1. Despite the fact that our analysis did not take into consideration the minor presence (10%) of the left over native MauG in the Ca^{2+}-depleted sample, the agreement between the experimental spectra and the simulated spectra of the major component (LS*) is reasonably good. In Table 1, the crystal field parameters, Δ/λ and V/Δ, for the low-spin heme derived from freezing of HS and for LS* calculated from the crystal field theory (*24*) are also listed, where Δ and V are the axial and rhombic crystal field parameters, respectively, and λ the spin orbit coupling constant.

Proton relaxometry

Proton NMR relaxometry was used to examine the conformational change of the hemes upon the depletion of calcium through the comparison of the relaxivity of native and Ca^{2+}-depleted MauG proteins (Figure S1, Supplemental Data). The relaxivity information obtained by this technique is different from the spin relaxivity retrieved through EPR spectroscopy. The purpose of doing this set of experiments was to obtain the information of the inner water molecules instead of the relaxivity of the hemes. The r_1 and r_2 values were calculated from eqs. 2 and 3 from the T_1 and T_2 values obtained from data fitting in Figure S1. A decrease of the r_1 and r_2 values of the Ca^{2+}-depleted MauG was observed. The r_1 value was changed from 1.359 ± 0.013 to 0.458 ± 0.002 $mM^{-1}s^{-1}$, while r_2 value changed from 3.915 ± 0.008 to 1.653 ± 0.004 $mM^{-1}s^{-1}$. The decrease of the r_1 and r_2 values suggests

that the removal of calcium changed the relaxation properties of the heme centers. As discussed later, the number of water molecules in the heme sites may have been altered due to departure of the Ca^{2+} ion.

Discussion

The calcium binding site in MauG is decidedly unusual, because the ligands do not consist of negatively charged residues such as Asp or Glu as commonly seen in the well-characterized Ca^{2+} binding sites of other proteins. Yet the calcium binding in MauG is relatively tight (K_d =5.3 μM) (*16*), suggesting that ligand charge is not the sole factor influencing binding affinity. When the Ca^{2+} ion is removed, the structural changes cause enzyme inactivation, implying notable alterations occurred at the heme centers. In this work, we conducted an extensive spectroscopic study comparing the Ca^{2+}-depleted MauG and the native enzyme. One of the two key findings in this work is that the presence or absence of Ca^{2+} in MauG exerts a significant influence on the magnetic properties of its two heme centers and the relative orientation of the heme axial ligands. The second key finding of this work is that the hemes become HALS-like species when Ca^{2+} is absent. A discussion of our results follows.

HALS-like hemes in Ca^{2+}-depleted MauG

Highly anisotropic low-spin (HALS) hemes have been known since the early work of Griffith (*27*, *28*), Blumberg and Peisach (*29*, *30*), Taylor (*31*), Bohan (*32*), Loew (*33*), Walker (*26*, *34*-*36*) and many others (for reviews see ref. (*35*, *37*, *38*)). In the 1970s, a “truth diagram” with the ligand field parameters was defined by Blumerg and Peisach to calculate the *g*-values. This diagram was experimentally examined on the ferric porphyrin complexes and proteins by Walker and many others (for reviews see ref. (*35*) and (*38*)). The EPR studies have provided a detailed picture of g_{max} and *g*-anisotropy in relation to the electronic structure of ferric porphyrins/hemes with highly axial or rhombic ligation of the heme axial ligands.

As described previously in this study, several independent spectroscopic techniques show that, upon the depletion of the Ca^{2+} ion, the two heme sites undergo a dramatic structural change even though the overall protein secondary structure is relatively unaltered (*16*). In Ca^{2+}-depleted MauG, over 90% of the enzyme is in the Ca^{2+}-free form. Other than the 10% of leftover native MauG EPR signals, the remaining 90% of ferric hemes in Ca^{2+}-depleted MauG are almost complete absent at the typical low microwave power conditions (Figure 2). The signal intensities only look comparable to those of native MauG at higher microwave power conditions (Figure 5). The two hemes in Ca^{2+}-free MauG have become spectroscopically indistinguishable from each other. The results of the multifrequency EPR and Mössbauer studies are consistent with significantly changed electromagnetic properties of the ferric hemes in Ca^{2+}-depleted MauG. These spectroscopic data also point to a very large g_{max} (g_x in this case) value and *g*-anisotropy ($g_x - g_z$) value in LS*, which suggest the formation of HALS heme species.

The hallmark of HALS is that its members present a very large g_{max} value (2.9 – 3.5) and *g*-anisotropy ($g_{max} - g_{min}$). The two hemes in Ca^{2+}-free MauG present as LS* species with similar EPR *g* values of 1.50, 2.27, and 2.97 and Mössbauer parameters (δ = 0.28 mm/s and ΔE_Q = 2.17 mm/s). As this g_{max} value is at the low end or what some might consider below the threshold for HALS, it is referred to as HALS-like. HALS species were divided into two subgroups by Walker (*35*). Their spectroscopic properties were elaborated very recently in a review by Andersson and co-workers (*38*). The highly axial systems present a perpendicular axial ligand plane (Type I) and the highly rhombic strained configuration systems are type II. Upon removal of Ca^{2+}, the structure of MauG changes such that the HS and LS hemes

are each converted to HALS-like species with highly rhombic EPR signals. In the case of the high-spin ferric heme, the change in EPR properties is associated with the introduction of a new axial ligand which converts the heme to a low-spin form. In the case of the native low-spin ferric heme, the His and Tyr axial ligands are retained but must undergo a change in orientation and bond angles relative to the heme and each other.

While the Ca^{2+}-depleted MauG has presumably two distinct sets of axial ligates in their HALS-like species, their EPR and Mössbauer parameters are nearly identical. This is not surprising since HALS and HALS-like, despite being ligated by different residues, are known to exhibit similar EPR and Mössbauer signals (Table 2). The EPR and Mössbauer parameters for Ca^{2+}-free MauG resemble those exhibited by HALS-like with *bis*-His, His-Met, and His-Tyr ligation (Table 2). The correlation of plane orientation of the axial ligand groups with *g* values has been established for *bis*-His and His-Met HALS (*38*). Such a structural correlation, however, has not been previously characterized for His-Tyr ligated hemes due to the existence of very few examples of the His-Tyr ligated hemes.

Estimation of the alteration of heme axial ligand orientation angles

We have utilized the crystal field theory and the “truth diagram” to estimate the axial ligand plane angles. The nature of rhombic versus axial in the ligand plane orientation of HALS is characterized by the crystal field parameter V/Δ . The value of V/Δ can be directly obtained from simulation of the Mössbauer data (Table 1). It can also be calculated from precisely determined principal *g* values by HFEPR according to eqs 4 and 5. For a completely axial system (type I), *i.e*. the two axial protein ligands are perpendicular with each other in terms of their planes (Figure 7), $V/\Delta \rightarrow 0$. For a pure rhombic system, V/Δ is assumed to be close to 0.67 (*38*).

$$\frac{V}{\xi}=\frac{g_x}{g_z+g_y}+\frac{g_y}{g_z-g_x} \tag{4}$$

$$\frac{\Delta}{\xi}=\frac{g_x}{g_z+g_y}+\frac{g_z}{g_y-g_x}-\frac{V}{2\xi} \tag{5}$$

We have attempted to interpret the EPR data by estimating the relative planar angles of the two aromatic rings of Tyr and His. The EPR and Mössbauer characterizations of those structurally defined systems, especially the single-crystal EPR studies, of HALS have suggested a pseudo-Jahn-Teller contribution to the crystal field, the magnitude of which depends on the orientation of the axial ligands (*36*, *39*, *40*). Quinn et al. characterized five synthesized *bis*-imidazole complexes by both X-ray crystallography and single-crystal EPR techniques (*40*). The results suggest a linear correlation of the experimental values of V/Δ and $\Delta\phi$ (*40*). Versed in the knowledge of such a linear relationship and the two sets of the theoretical data V/Δ (0, 0.67) and the corresponding $\Delta\phi$ (90° and 0°, respectively), we formulated the following new equation for axial ligand plane angle estimations:

$$\Delta\phi = (0.67000 - V/\Delta)/0.00744 \tag{6}$$

When data points of reference (*40*) were fitted, a similar equation was obtained (eq 7). While this equation is more pertinent to *bis*-imidazole complexes and the *bis*-His ligated biological heme centers-it was of interest to apply it to the original five-coordinate HS data for Ca^{2+}-depleted MauG.

$$\Delta\phi = (0.70765 - V/\Delta)/0.00547 \quad (7)$$

The difference between eqs 6 and 7 are likely due to one of the axial ligands not being aligned in the straight axial position but instead bent with an angle even though the phenolate oxygen is always in the plane defined by the phenol ring of Tyr for the His-Tyr heme. Also, the crystal field parameters calculated from equations (4) and (5) are slightly different than those obtained from Griffith's crystal field theory (*41*) because eqs 4 and 5 are approximation of Griffith's theorem (*41*). From eqs 4 and 5, we calculated the value of V/Δ from HFEPR for the new LS*. This number is 0.566 (g_x = 1.50, g_y = 2.27, g_z = 2.97), which is approximately the same as that obtained from Mössbauer spectroscopy, 0.55 (Table 1). When the V/Δ value is plugged into eq 6, the calculated Δϕ value is 14° (EPR) or 16° (Mössbauer spectroscopy), which is consistent with a more rhombic axial ligand plane. When eq 7 is used, the calculated Δϕ value is 26° (from EPR data) or 29° (from Mössbauer data). Given these results one may conservatively estimate that the angles of the axial heme ligand planes for the LS* species are between 14° and 29° (or 21° ± 8°). This range is consistent with that of the so-called type II HALS (for a recent review see ref. (*38*)) (Figure 7). The EPR and Mössbauer data led to very similar ligand orientation angle estimations (with only 2° - 3° difference). It should be kept in mind that the LS* species is actually two different hemes with indistinguishable properties. The estimation of relative plane angle for LS* would not be applicable to the His-Tyr heme site, because the flexibility of the Tyr coordination to the Fe ion can stray from the axial position and deviate an angle at the point of the phenolic oxygen. Although the actual Δϕ value in the His-Tyr heme site cannot be estimated from the above equations, the large g_{max} value and *g*-anisotropy suggest a significant conformational change of Δϕ in Ca^{2+}-free MauG, from 72° to a more rhombic ligand plane.

It should be noted that the Δϕ value of the original LS in native MauG cannot be calculated from eqs. 6 and 7, because LS in native MauG is not a HALS-like species. Fortunately, it can be obtained from the crystal structure of MauG-preMADH complex. The Tyr ligand in the six-coordinate heme is not perpendicular to the heme plane (*12*). It is inclined from the anticipated axial position. Using the Discovery Studio Visualizer Client 3.0 program from Accelrys, the heme plane angle was measured to be 72°. Thus, the conversion of the LS heme to LS* heme is consistent with a dramatic change in the relative orientations of the His and Tyr heme ligands with respect to each other. It should be emphasized, however, that the angle calculations presented here are intended to be a qualitative argument rather than as quantitative because of approximations described above.

Why is Ca^{2+}-depleted MauG inactive?

When the chemical nature of the heme centers is unraveled, we are no longer puzzled by the mystery of the enzyme inactivation in MauG associated with depletion of the Ca^{2+} ion. Although two hemes are present in MauG, only one of them reacts with external oxidant. The originally five-coordinate (5C, His-ligated) HS heme site is known to be the reactive site with oxidant and the six-coordinate (6C, His-Tyr ligated) LS heme shares electrons and charges with the 5C heme (20). The 5C ferric heme reacts with hydrogen peroxide and initially generates a ferryl and a cation radical. The radical immediately oxidizes the 6C heme and generates a *bis*-Fe(IV) heme (*17*). At the reduced state, the 5C ferrous heme reacts with CO, NO and presumably O_2 while the His-Tyr ligated heme is inaccessible to external small molecules (*42*). These conclusions were obtained in our previous biochemical and EPR study and recently confirmed by X-ray crystallography (*43*). Upon removal of the Ca^{2+} ion, we found that the 5C HS heme is present as a 6C HALS-like species. In the Ca^{2+}-

depleted MauG, the H_2O_2 binding site is occupied by an amino acid residue or a solvent derived molecule from the protein so that the enzyme is not catalytically active.

At the originally five-coordinate (5C) heme site, the identity of the new axial sixth heme ligand that converts the HS heme to a LS* heme is not known. In *P. nautica* CcP, the 5C heme picks up a distal His71 and generates a *bis*-His ligated LS heme. It is not clear if the structurally characterized *P. nautica* CcP *bis*-His ligated LS heme is a HALS species, but the *bis*-His in *Paracoccus denitrificans* CcP is HALS-like (Table 2). The corresponding His71 is not found in the MauG sequence. Instead, A Met (residue 114 in MauG or 115 in some of the other family members) is conserved over the broader group of sequences, which may be an alternative distal heme ligand in Ca^{2+}-free MauG. Inspection of the crystal structure of native MauG for nearby residues reveals that Asp, Glu and Met, but not His residues, could potentially provide a heme ligand. These residues are within 10 Å of the heme Fe ion in the distal pocket of the 5C HS heme. Barring a major structural rearrangement it is not likely for His-His ligation to occur in the HALS-like species in MauG. Previous circular dichroism and resonance Raman studies, however, did not support a major structural rearrangement (*16*). Unfortunately, it is not yet possible to crystallize Ca^{2+}-depleted MauG. Identification of the added sixth ligand to the 5C HS heme upon removal of Ca^{2+} in MauG will be the subject of future study. On the basis of the available information, it seems most likely that a Met residue is repositioned and provides the distal axial ligand in the Ca^{2+}-free MauG.

The freezing effect

As has been reported earlier, upon freezing the native enzyme, a fraction of the HS ferric heme, is converted to low-spin (*17*). This is not a problem in this study because the 5C heme has already been converted to a 6C ferric heme species during the depletion of Ca^{2+} from MauG. However, such a cooling effect does cause complication when comparing the data of Ca^{2+}-depleted MauG with that obtained from native MauG. About half of the originally 5C HS heme in native MauG (the control sample), or 25% of the total heme, becomes a LS heme upon freezing the concentrated samples. Such a high-to-low-spin transition upon cooling the enzyme is known in other diheme enzymes. For example, the HS heme in oxidized *P. denitrificans* CcP nearly completely converts to LS heme upon being frozen (*44*, *45*). *P. denitrificans* CcP and MauG are closely related periplasmic proteins. The two enzymes share a noticeable amino acid sequence similarity (15). The LS Heme generated by cooling in the two diheme enzymes also show nearly identical spectroscopic properties.

The EPR and Mössbauer parameters for the artifactual LS species derived from the freezing effect in both native MauG and *P. denitrificans* CcP are very similar to those of the LS* species in Ca^{2+}-free MauG, although not identical. This suggests that structural changes at the originally HS site of native MauG occurring during freezing may be similar to those that occur during Ca^{2+} removal in solution. A water molecule is located about 3.7 - 3.8 Å away from the HS heme in two copies of the native MauG crystal structure. A similar water molecule is present in the distal pocket of the 5C heme in bacterial diheme CcP structures (PDB entries: 1rz5 and 2vhd). The water molecule is likely the candidate to ligate to the 5C heme during the cooling process. An experimentally relevant piece of information is the proton relaxivity study which suggests that the removal of Ca^{2+} alters the inner phase water content of MauG. The decrease in the values of the relaxivity parameters observed in the proton relaxation experiments is consistent with three possibilities. First, spin quantum number (S) directly contributes to the longitudinal (T_{1m}) and transverse relaxation time (T_{2m}) of bonded water according to the equations included in the supporting information section. The EPR/Mössbauer data show that the removal of calcium causes a spin state change of one of the hemes from 5/2 to 1/2. This should increase both T_{1m} and T_{2m} (eqs S1 & S2, supporting information), which is consistent with the observation of decreased r_1 and

r_2 values of the heme (eqs. S3 and S4, supporting information). Second, the relaxivity parameters of r_1 and r_2 are a function of *n*, *i.e*., the number of water ligands present in the first coordination shell. The observed decrease in both relaxivity parameter values may well indicate decrease in the number of water molecules near iron ions upon the removal of calcium. Third, it is also possible but less likely that the removal of calcium results in the change of τ_c, the effective dipolar correlation time (eqs S1-S4) as seen in the characterization of phenylalanine hydroxylase (*46*).

The role of Ca^{2+} ion

We have learned from our previous study that the two heme centers in native MauG must efficiently share electrons so that the critical *bis*-Fe(IV) intermediate is formed when the five-coordinate heme reacts with H_2O_2 (*17*, *42*). In the absence of the Ca^{2+} ion, there is no evidence so far that the *bis*-Fe(IV) state of MauG could be formed in the absence of the Ca^{2+} ion, implying that the communication between the two iron ions is obstructed due to the departure of the Ca^{2+} ion. Thus, a role of Ca^{2+} in MauG is to maintain an environment that facilitates the electronic communication with the catalytic diheme center. In other words, a proper conformation of the enzyme active site and its rigidity depend on the presence of Ca^{2+} ion. It seems only possible with the Ca^{2+} ion bound in the proximity of the two hemes, that the Fe ions will efficiently share electrons during the catalytic cycle without spin coupling.

In most of the as-isolated bacterial diheme CcPs, the H_2O_2-binding heme is blocked by the presence of a distal His ligand. So the His-His ligated heme is not reactive to external small oxidants. The reduction of the other His-Met heme generates a mixed-valence state that triggers a Ca^{2+}-dependent conformational change in which the distal His is replaced by water and hence becomes reactive towards H_2O_2. The mixed-valent Fe(II)-Fe(III) state is stable is CcPs because the redox potentials of the two hemes are widely separated by several hundred millivolts. In contrast, the intrinsic redox potentials of the two hemes of MauG are similar and so the hemes are oxidized and reduced simultaneously with no formation of a mixed valence state (*42*). This highlights the fact that in CcPs, Ca^{2+} plays an important role in the regulation of activity by interconverting the enzyme between an inactive diferric state and an active mixed valence state. This is not the role of Ca^{2+} in MauG, as it is active in the diferric state and does not exhibit a mixed valence state under any conditions. A regulatory role of Ca^{2+} in MauG cannot be ruled out because the changes in spectroscopic properties and enzymatic activity caused by removal of Ca^{2+} are reversed by re-addition of Ca^{2+}. However, as a reductant is not required for Ca^{2+} binding it seems unlikely that Ca^{2+} would dissociate in the absence of chelators in its physiological localization in the periplasm.

Summary

Calcium plays a wide range of vital roles in proteins. The ability to catalyze TTQ biosynthesis and the magnetic properties of the two hemes of MauG are significantly altered by the removal from MauG of a relatively tightly bound Ca^{2+}. Interestingly, these changes are reversible with the back addition of $CaCl_2$. Both the five-coordinate high-spin heme and six-coordinate low-spin heme are converted to highly rhombic low-spin hemes with similar electronic properties in the Ca^{2+}-depleted MauG. This is caused by introduction of a sixth ligand to the high-spin heme and reorientation of the His and Tyr axial ligands of the low-spin heme. In the Ca^{2+}-free form, the two ferric hemes are present as HALS-like species with highly rhombic axial ligands. Mössbauer spectroscopic data rule out the possibility of a direct spin-coupling between the two hemes. The relaxation properties of the hemes in Ca^{2+}-depleted MauG are changed with a much increased half power saturation value. Depletion of Ca^{2+} also reduces both r_1 and r_2 relaxivity values consistent with a loss of inner phase water molecules which may explain the effects of Ca^{2+} on both hemes since it is connected to each

by structural water networks. Thus, we conclude that the tightly-bound Ca^{2+} of MauG profoundly influences the axial ligation geometry and magnetic properties of the catalytic diheme center. It is quite remarkable that depletion of Ca^{2+} so dramatically alters the chemical and magnetic properties of both hemes of MauG as well as changes the axial ligand orientations and that this alteration is reversible. Overall this work provides a new example of protein-bound HALS-like hemes and a novel mechanism by which Ca^{2+} influences the protein structure to support the catalytic activity of a metalloenzyme. Moreover, this work also provides an example of a spectroscopically characterized His-Tyr ligated heme.

Supplementary Material

Refer to Web version on PubMed Central for supplementary material.

Acknowledgments

We thank Dr. Boi Hanh (Vincent) Huynh of Emory University for access to Mössbauer spectroscopy and his invaluable guidance in data analyses. We acknowledge Dr. Andrew Ozarowski for his EPR simulation program SPIN. HFEPR studies were supported by the National High Magnetic Field Laboratory, which is funded by the NSF through Cooperative Agreement DMR 0654118, the State of Florida, and the DOE.

ABBREVIATIONS

EPR	electron paramagnetic resonance
HFEPR	high frequency/high field EPR
CcP	cytochrome *c* peroxidase
5C	five-coordinate
6C	six-coordinate
HS	high-spin
LS	low-spin
LS*	a low-spin ferric ion with large *g*-anisotropy
HALS	highly anisotropic/highly axial low-spin
preMADH	precursor of methylamine dehydrogenase
TTQ	tryptophan tryptophylquinone

REFERENCES

1. Forsen, SK. J. Calcium in biological systems. In: Bertini, I.; Gray, B.; Lippard, SJ.; Valentine, JS., editors. Bioinorganic Chemistry. University Science Books; Mill Valley, CA: 1994.
2. Heizmann CWB,K. Changes in Ca^{2+}-binding proteins in human neurodegenerative disorders. Trends Neurosci. 1992; 15:259–264. [PubMed: 1381122]
3. Kretsinger RH. Calcium coordination and the calmodulin fold: divergent versus convergent evolution. Cold Spring Harb. Symp. Quant. Biol. 1987; 52:499–510. [PubMed: 3454274]
4. Nishizuka Y. Calcium, phospholipid turnover and transmembrane signalling. Philos. Trans. R Soc Lond B Biol. Sci. 1983; 302:101–112. [PubMed: 6136998]
5. Dennis EA. The growing phospholipase A2 superfamily of signal transduction enzymes. Trends Biochem. Sci. 1997; 22:1–2. [PubMed: 9020581]
6. Obeta JAN, Okungbowa J, Ezeogu LI. Malting of sorghum: further studies on factors influencing α-amylase activity. J. Institute Brewing. 2000; 106:295–304.

7. Nikonava LV, Nanazashvili MG, Krotova KE, Nazarova LF, Rabaya NA, Prusakova OV, Beletskii IP. Comparative study of Ca/Mg-dependent nucleases of the mammalian thymus *Izv*. Akad. Nauk. Ser. Biol. 1998; 2:180–186.
8. Dennis J,S. Mammalian nitric oxide synthases. Biochim. Biophys. Acta. 1999; 1411:217–230. [PubMed: 10320659]
9. Dias JM, Alves T, Bonifácio C, Pereira AS, Trincão J, Bourgeois D, Moura I, Romão MJ. Structural basis for the mechanism of Ca^{2+} activation of the di-Heme cytochrome c peroxidase from *Pseudomonas nautica* 617. Structure. 2004; 12:961–973. [PubMed: 15274917]
10. Lopes H, Pettigrew GW. Electrochemical study on cytochrome *c* peroxidase from *Paracoccus denitrificans*: a shifting pattern of structural and thermodynamic properties as the enzyme is activated. J. Biol. Inorg. Chem. 1998; 3:632–642.
11. Wang Y, Graichen ME, Liu A, Pearson AR, Wilmot CM, Davidson VL. MauG, a novel diheme protein required for tryptophan tryptophylquinone biogenesis. Biochemistry. 2003; 42:7318–7325. [PubMed: 12809487]
12. Jensen LMR, Sanishvili R, Davidson VL, Wilmot CM. In crystallo posttranslational modification within a MauG/pre-methylamine dehydrogenase complex. Science. 2010; 327:1392–1394. [PubMed: 20223990]
13. Li X, Jones LH, Pearson AR, Wilmot CM, Davidson VL. Mechanistic possibilities in MauG-dependent tryptophan tryptophylquinone biosynthesis. Biochemistry. 2006; 45:13276–13283. [PubMed: 17073448]
14. Pearson AR, De la Mora-Rey T, Graichen ME, Wang Y, Jones LH, Marimanikkupam S, Agger SA, Grimsrud PA, Davidson VL, Wilmot CM. Further insights into quinone cofactor biogenesis: Probing the role of *mauG* in methylamine dehydrogenase tryptophan tryptophylquinone formation. Biochemistry. 2004; 43:5494–5502. [PubMed: 15122915]
15. Davidson VL. Pyrroloquinoline quinone (PQQ) from methanol dehydrogenase and tryptophan tryptophylquinone (TTQ) from methylamine dehydrogenase. Adv. Protein Chem. 2001; 58:95–140. [PubMed: 11665494]
16. Shin S, Feng M, Chen Y, Jensen LM, Tachikawa H, Wilmot CM, Liu A, Davidson VL. The tightly bound calcium of MauG is required for tryptophan tryptophylquinone cofactor biosynthesis. Biochemistry. 2011; 50:144–150.
17. Li X, Fu R, Lee S, Krebs C, Davidson VL, Liu A. A catalytic di-heme *bis*-Fe(IV) intermediate, alternative to an Fe(IV)=O porphyrin radical. Proc. Natl. Acad. Sci. U.S.A. 2008; 105:8597–8600. [PubMed: 18562294]
18. Tarboush NA, Jensen LMR, Feng M, Tachikawa H, Wilmot CM, Davidson VL. Functional importance of tyrosine 294 and the catalytic selectivity for the bis-Fe(IV) state of MauG revealed by replacement of this axial heme ligand with histidine. Biochemistry. 2010; 49:9783–9791. [PubMed: 20929212]
19. Ozarowski A, Lee HM, Balch AL. Crystal environments probed by EPR spectroscopy. Variations in the EPR spectra of Co(II)(octaethylporphyrin) doped in crystalline diamagnetic hosts and a reassessment of the electronic structure of four-coordinate cobalt(II). J. Am. Chem. Soc. 2003; 125:12606–12614. [PubMed: 14531705]
20. Portis AM. Electronic structure of F centers: Saturation of the electron spin resonance. Phys. Rev. 1953; 91:1071–1078.
21. Castner. Saturation of the paramagnetic resonance of a V center. Phys. Rev. 1959; 115:1506–1515.
22. Galli C, Innes JB, Hirsh DJ, Brudvig GW. Effects of dipole-dipole interactions on microwave progressive power saturation of radicals in proteins. J. Magn. Res. 1996; B110:284–287.
23. Hassan AK, Pardi LA, Krzystek J, Sienkiewicz A, Goy P, Rohrer M, Brunel LC. Ultrawide band multifrequency high-field EMR technique: A methodology for increasing spectroscopic information. J. Magn. Reson. 2000; 142:300–312. [PubMed: 10648147]
24. Griffith JS. Theory of EPR in low-spinferric hemoproteins. Mol. Phys. 1971; 21:135–139.
25. Oosterhuis WT, Lang G. Mössbauer effect in potassium hexacyanoferrate(III). Phys. Rev. 1969; 178:439–456.

26. Walker FA, Huynh BH, Scheidt WR, Osvanth SR. Models of the cytochromes *b*. Effect of axial ligand plane orientation on the EPR and Mössbauer spectra of low-spin ferrihemes. J. Am. Chem. Soc. 1986; 108:5288–5297.
27. Griffith JS. The magnetic properties of some hemoglobin complexes. Proceedings of the Royal Society of London, Series A: Mathematical, Physical and Engineering Sciences. 1956; 235:23–36.
28. Griffith JS. Theory of EPR in low-spin ferric hemoproteins. Mol. Phys. 1971; 21:135–139.
29. Blumberg, WE.; Peisach, J. Chance, B.; Yonetani, T.; Mildvan, AS., editors. Probes and Structure and Function of Macromolecules and Membranes. 1971. p. 215-229.
30. Peisach J, Blumberg WE, Adler A. Electron paramagnetic resonance studies of iron porphin and chlorin systems. Ann. N. Y. Acad. Sci. 1973; 206:310–327. [PubMed: 4356182]
31. Taylor CPS. The EPR of low spin heme complexes. Relation of the t2g hole model to the directional properties of the *g* tensor, and a new method for calculating the ligand field parameters. Biochim. Biophys. Acta. 1977; 491:137–149. [PubMed: 191085]
32. Bohan TL. Analysis of low-spin ESR spectra of ferric heme proteins: a reexamination. J. Magn. Reson. 1977; 26:109–118.
33. Loew GH. Analysis of the electron spin resonance of low spin ferric heme compounds. Biophys. J. 1970; 10:196–212. [PubMed: 4313212]
34. Raitsimring AM, Borbat P, Shokhireva TK, Walker FA. Magnetic field (*g*-Value) dependence of proton hyperfine couplings obtained from ESEEM measurements: Determination of the orientation of the magnetic axes of model heme complexes in glassy media. J. Phys. Chem. 1996; 100:5235–5244.
35. Walker FA. Magnetic spectroscopic (EPR, ESEEM, Mössbauer, MCD and NMR) studies of low-spin ferriheme centers and their corresponding heme proteins. Coord. Chem. Rev. 185. 1999; 186:471–534.
36. Walker FA. The heme environment of mouse neuroglobin: histidine imidazole plane orientations obtained from solution NMR and EPR spectroscopy as compared with X-ray crystallography. J. Biol. Inorg. Chem. 2006; 11:391–397. [PubMed: 16586113]
37. Walker FA. Models of the bis-histidine-ligated electron-transferring cytochromes. Comparative geometric and electronic structure of low-spin ferro- and ferrihemes. Chem. Rev. 2004; 104:589–615. [PubMed: 14871136]
38. Zoppellaro G, Bren KL, Ensign AA, Harbitz E, Kaur R, Hersleth H-P, Ryde U, Hederstedt L, Andersson KK. Studies of ferric heme proteins with highly anisotropic/highly axial low spin (*S* = 1/2) electron paramagnetic resonance signals with bishistidine and histidine-methionine axial iron coordination. Biopolymers. 2009; 91:1064–1082. [PubMed: 19536822]
39. Byrn MP, Katz BA, Keder NL, Levan KR, Magurany CJ, Miller KM, Pritt JW, Strouse CE. Low-spin ferric porphyrin complexes: analysis of the electronic structure based on single-crystal electron spin resonance measurements. J. Am. Chem. Soc. 1983; 105:4916–4922.
40. Quinn R, Valentine JS, Byrn MP, Strouse CE. Electronic structure of low-spin ferric porphyrins: a single-crystal EPR and structural investigation of the influence of axial ligand orientation and the effects of pseudo-Jahn-Teller distortion. J. Am. Chem. Soc. 1987; 109:3301–3308.
41. Griffith, JS. The Theory of Transition-Metal Ions. Cambridge University Press; Cambridge: 1964.
42. Fu R, Liu F, Davidson VL, Liu A. Heme iron nitrosyl complex of MauG reveals an efficient redox equilibrium between hemes with only one heme exclusively binding exogenous ligands. Biochemistry. 2009; 48:11603–11605. [PubMed: 19911786]
43. Yukl ET, Goblirsch BR, Davidson VL, Wilmot CM. Crystal structures of CO and NO adducts of MauG in complex with pre-methylamine dehydrogenase: Implications for the mechanism of dioxygen activation. Biochemistry. 2011; 50:2931–2938. [PubMed: 21355604]
44. Gilmour R, Goodhew CF, Pettigrew GW, Prazeres S, Moura I, Moura JJG. Spectroscopic characterization of cytochrome *c* peroxidase from *Paracoccus denitrificans*. Biochem. J. 1993; 294:745–752. [PubMed: 8397509]
45. Prazeres S, Moura JJG, Moura I, Gilmour R, Goodhew CF, Pettigrew GW, Ravi N, Huynh BH. Mössbauer characterization of *Paracoccus denitrificans* cytochrome *c* peroxidase - Further evidence for redox and calcium binding-induced heme-heme interaction. J. Biol. Chem. 1995; 270:24264–24269. [PubMed: 7592634]

46. Olafsdottir S, Martínez A. The accessibility of iron at the active site of recombinant human phenylalanine hydroxylase to water as studied by ^{1}H NMR paramagnetic relaxation. Effect of L-Phe and comparison with the rat enzyme. J. Biol. Chem. 1999; 274:6280–6284. [PubMed: 10037716]
47. Huynh BL, Emptage MH, Munck E. Mössbauer study of cytochrome c2 from *Rhodospirillum rubrum*. Sign of the product gxgygz of some low spin ferric heme proteins. Biochim. Biophys. Acta. 1978; 534:295–306. [PubMed: 208633]
48. Grein F, Venceslau SS, Schneider L, Hildebrandt P, Todorovic S, Pereira IA, Dahl C. DsrJ, an essential part of the DsrMKJOP transmembrane complex in the purple sulfur bacterium *Allochromatium vinosum*, is an unusual triheme cytochrome *c*. Biochemistry. 2010; 49:8290–8299. [PubMed: 20726534]
49. Cheesman MR, Ferguson SJ, Moir JW, Richardson DJ, Zumft WG, Thomson AJ. Two enzymes with a common function but different heme ligands in the forms as isolated. Optical and magnetic properties of the heme groups in the oxidized forms of nitrite reductase, cytochrome cd1, from *Pseudomonas stutzeri* and *Thiosphaera pantotropha*. Biochemistry. 1997; 36:16267–16276. [PubMed: 9405061]
50. Pipirou Z, Bottrill AR, Svistunenko DA, Efimov I, Basran J, Mistry SC, Cooper CE, Raven EL. The reactivity of heme in biological systems: autocatalytic formation of both tyrosine-heme and tryptophan-heme covalent links in a single protein architecture. Biochemistry. 2007; 46:13269–13278. [PubMed: 17958400]
51. Nicoletti FP, Howes BD, Fittipaldi M, Fanali G, Fasano M, Ascenzi P, Smulevich G. Ibuprofen induces an allosteric conformational transition in the heme complex of human serum albumin with significant effects on heme ligation. J. Am. Chem. Soc. 2008; 130:11677–11688. [PubMed: 18681435]
52. Echalier A, Brittain T, Wright J, Boycheva S, Mortuza GB, Fulop V, Watmough NJ. Redox-linked structural changes associated with the formation of a catalytically competent form of the diheme cytochrome *c* peroxidase from *Pseudomonas aeruginosa*. Biochemistry. 2008; 47:1947–1956. [PubMed: 18217775]
53. Ravi N, Moura I, Costa C, Teixeira M, LeGall J, Moura JJ, Huynh BH. Mössbauer characterization of the tetraheme cytochrome c3 from *Desulfovibrio baculatus* (DSM 1743). Spectral deconvolution of the heme components. Eur. J. Biochem. 1992; 204:779–782. [PubMed: 1311680]
54. Safo MKG, G. P, Walker FA, Scheidt WR. Models of the cytochromes *b*. Control of axial ligand orientation with a hindered porphyrin system. J. Am. Chem. Soc. 1991; 113:5497.
55. Teschner T, Yatsunyk L, Schunemann V, Paulsen H, Winkler H, Hu CJ, Scheidt WR, Walker FA, Trautwein AX. Models of the membrane-bound cytochromes: Mössbauer spectra of crystalline low-spin ferriheme complexes having axial ligand plane dihedral angles ranging from 0 degrees to 90 degrees. J. Am. Chem. Soc. 2006; 128:1379–1389. [PubMed: 16433558]
56. Kessler DL, Rajagopalan KV. Purification and properties of sulfite oxidase from chicken liver. Presence of molybdenum in sulfite oxidase from diverse sources. J. Biol. Chem. 1972; 247:6566–6573. [PubMed: 4342603]

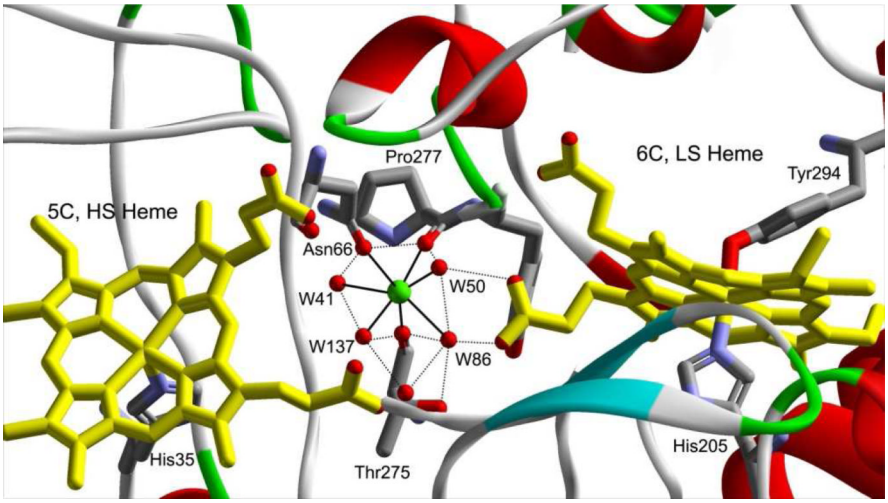

Figure 1.

The structure of the calcium binding site, 5-coordinate high-spin (5C, HS) and the 6-coordinate low-spin (6C, LS) hemes in MauG (PDB entry: 3l4m) (*12*). The H-bond network around the Ca^{2+} ion is shown in dotted line. For clarity, Trp93 and loops in front of the Ca^{2+} ion and hemes are omitted from this representation. “W” designates water molecules.

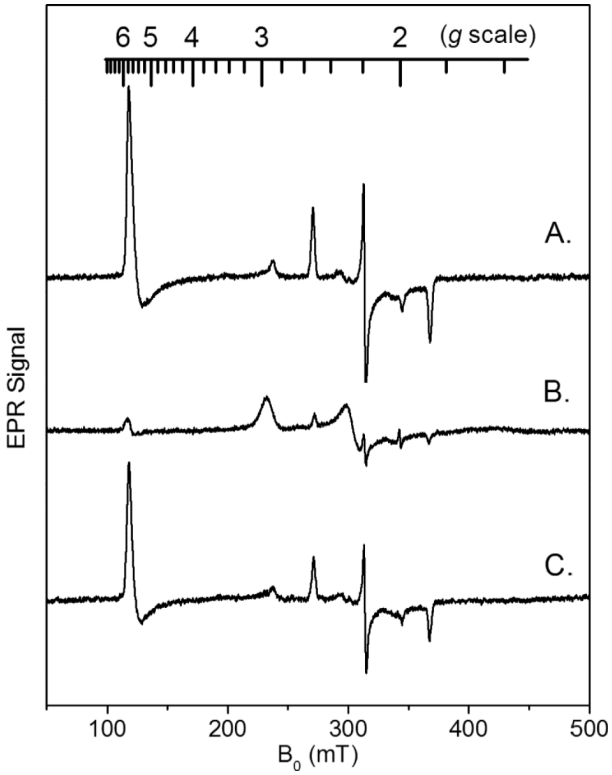

Figure 2.

X-band EPR spectra of MauG (A), Ca^{2+}-depleted MauG (B), and the Ca^{2+}-depleted MauG which was reconstituted with Ca^{2+} (C). EPR conditions: temperature 10 K, microwave frequency 9.6 GHz, microwave power 1 mW, and scan time 160 s. The *g*-scale is shown on the top of the figure.

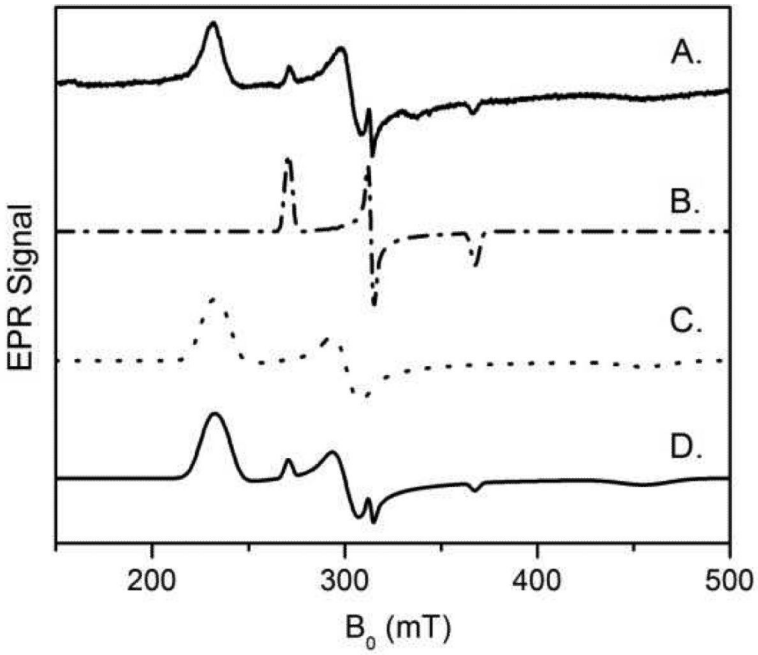

Figure 3.

EPR simulation of low-spin ferric hemes in the Ca^{2+}-depleted MauG. (A) The experimental spectrum obtained at 10 K with 1 mW microwave power, (B) simulated LS species, (C) simulated LS* species, and (D) Simulated spectrum with 0.1 LS and 0.9 LS*.

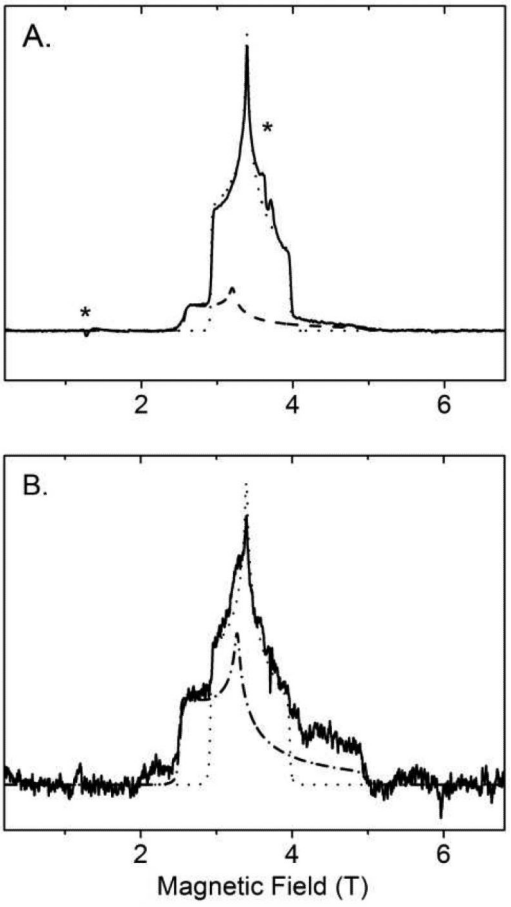

Figure 4.

High-field and high-frequency (104 GHz) EPR spectra of native (panel A) and Ca2+-depleted MauG (panel B) at 5 K with simulations. The HS heme is indicated by stars. The experimental data are shown in solid lines. The dotted line is the simulation of the LS heme in native MauG with *g* values of 2.545, 2.19, 1.873; the dashed line (2.89, 2.32, 1.50) in panel A presents the LS heme in native MauG derived from the high-spin heme upon freezing; The dash dotted line in panel B presents the newly formed LS* heme in the Ca^{2+}-depleted MauG with the *g* values of 2.97, 2.27, 1.50.

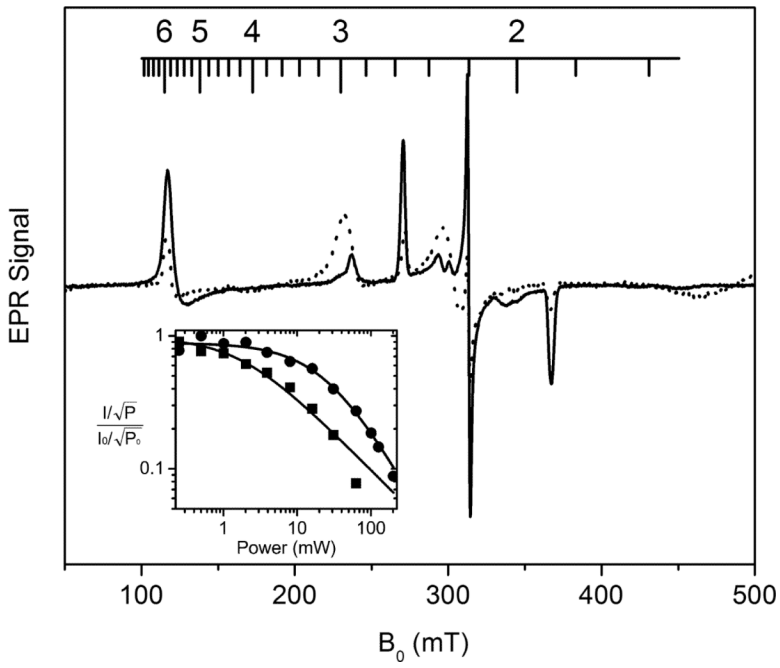

Figure 5.

X-band EPR spectra of native (dotted trace) and Ca^{2+}-depleted MauG (solid trace) taken at 10 K. These spectra were taken with identical instrument parameters with the exception that the former was obtained with 1 mW microwave power and the latter 12.7 mW. The inset is a plot of the 10 K power saturation profiles of the major low-spin ferric heme EPR signal in native (circles) and Ca^{2+}-depleted MauG (squares), respectively.

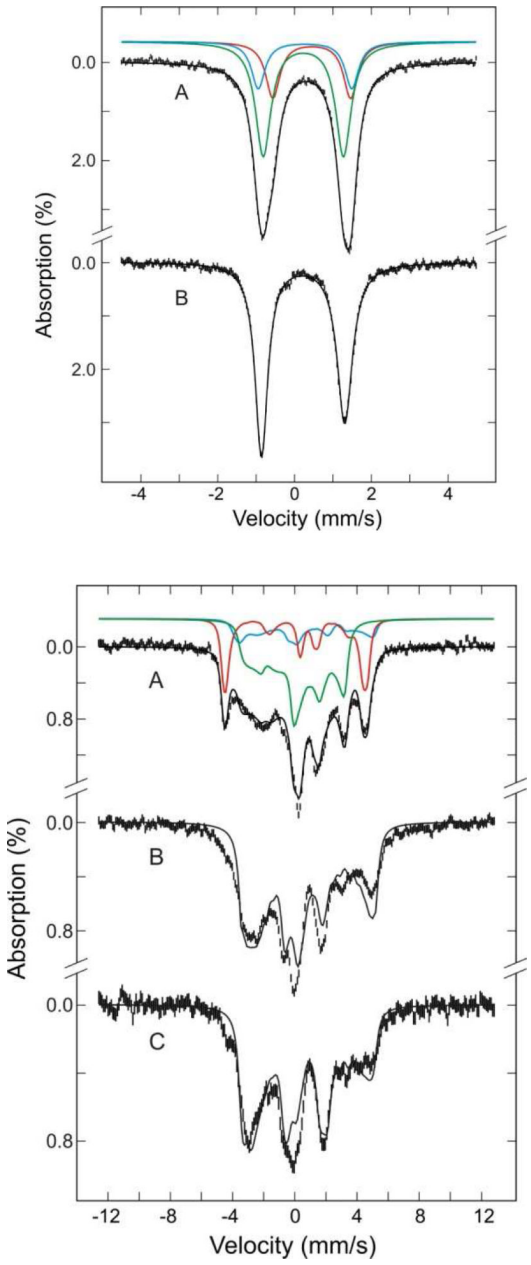

Figure 6.

Top panel: Mössbauer spectra of the native ^{57}Fe-MauG (A) and Ca^{2+}-depleted MauG (B) samples recorded at 180 K with a field of 50 mT parallel to the γ-radiation. The solid black line overlaid on the experimental data (vertical bars) is the composite simulation. The spectrum A consists of high-spin (red line) and low-spin (green and cyan lines) ferric heme moieties. The spectrum B is simulated with only low-spin ferric heme. The parameters and the percent components of each Fe-species are described in the text. Bottom panel: Mössbauer spectra of the ^{57}Fe-MauG (A) and Ca^{2+}-depleted MauG (B, C) samples recorded at 4.2 K in a field of 50 mT–parallel (A, B) and perpendicular (C) to the γ radiation. The solid black line overlaid on the experimental spectrum (vertical bars) is the composite simulation. The spectrum A is simulated with a high-spin (red line) and two low-spin (green

and cyan lines) ferric hemes. The spectrum B and C are simulated with only low-spin ferric heme.

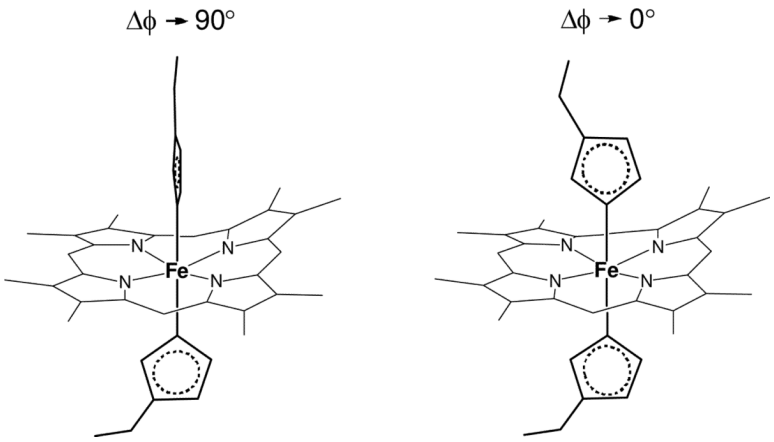

Figure 7.

A cartoon illustration of the relative axial ligand plane angles in extreme HALS and HALS-like species using ferric hemes with two axial histidine ligands as an example.

Table 1

Mössbauer and spin Hamiltonian parameters of the high- and low-spin ferric hemes in native and Ca^{2+}-depleted MauG

	Native MauG Hemes			Ca^{2+}-depleted MauG hemes
	HS[a]	**LS**[a]	**LS**[b]	**LS***
D[c] (cm^{-1})	10			
E/D [c]	0			
Δ/λ[c]			2.95	3.43
V/Δ[c]			0.68	0.55
g_x	5.57	1.87	1.52	1.52
g_y	1.99	2.19	2.32	2.27
g_z	1.99	2.54	2.89	2.97
$A_x/g_n/\beta_n$ (T)	–18.0	–35.0	–38.7	–32.0
$A_y/g_n\beta_n$ (T)	–18.0	9.30	22.6	15.0
$A_z/g_n\beta_n$ (T)	–18.0	29.4	50.6	50.0
ΔE_Q (mm/s)	2.0	2.09	2.44[d]	2.17[d]
δ (mm/s)	0.50	0.25	0.33	0.28
η [e]	0.4	–3.0	–3.0	–2.0

[a] The His-Tyr heme

[b] Low-spin species derived from freezing of the HS heme

[c] Δ and V are the axial and rhombic crystal field parameters and λ is the spin-orbit coupling constant; D is zero-field splitting; E/D is rhombicity parameter; $A_n/g_n\beta_n$ is the saturation field

[d] value at 180 K

[e] $\eta = (V_{xx} - V_{yy})/ V_{zz}$, where V_{ii} values are the principle components of the electric field gradient tensor.

Table 2

Comparison of EPR and Mössbauer parameters for the LS* hemes of Ca^{2+}-depleted MauG with those of HALS and HALS-like ferric heme species

	Principal *g* factor (g_x, g_y, g_z)	**Mössbauer parameters (mm/s)**	
Species		**Δ E_Q**	**δ**
Ca^{2+}-depleted MauG LS* hemes	2.97, 2.27, 1.52	2.17	0.28
His-Met ligated hemes			
P. denitrificans CcP (*45*)	3.41 (g_{max})	2.01	0.24
Cytochrome c_2 (*R. rubrum*) (*47*)	3.13, 2.11, 1.23	2.26	0.31
DsrMKJOP transmembrane complex cytochrome *c* (*Allochromatium vinosum*) (*48*)	2.96, 2.26, 1.50	N/A[1]	N/A
Ps. stutzeri cytocherome *cd*1, heme *c* (*49*)	2.997, 2.275, 1.4	N/A	N/A
His-Tyr ligated hemes			
Ascorbate peroxidase S160Y mutant (*50*)	2.94, 2.27,1.47	N/A	N/A
Heme-HAS-Ibuprofen complex (*51*)	2.93, 2.27,1.55	N/A	N/A
His-His ligated hemes			
P. denitrificans CcP (*45*)	2.89, 2.32, 1.51	2.52	0.31
P. aeruginosa CcP (*52*)	2.96, 2.27, 1.49	N/A	N/A
cytochrome *c3* (*D. baculutus*) (*53*)	2.93, 2.26, 1.51	2.0	0.24
$[(TMP)Fe(1\text{-}MeIm)2]^+$ (models of bis-histidinecoordinated cytochromes) (*54*, *55*)	2.886, 2.325, 1.571	2.14	0.27
Sulfite oxidase heme (*56*)	2.92, 2.25, 1.533	N/A	N/A

[1] N/A: not available